JOURNAL OF APPLIED PHYSICS **113**, 184903 (2013)

Chemo-mechanical softening during *in situ* nanoindentation of anodic porous alumina with anodization processing

Chuan Cheng[a] and A. H. W. Ngan
Department of Mechanical Engineering, The University of Hong Kong, Pokfulam Road, Hong Kong

(Received 22 December 2012; accepted 18 April 2013; published online 8 May 2013)

Simultaneous application of mechanical stresses on a material as it undergoes an electrochemical reaction can result in interesting coupling effects between the chemical and mechanical responses of the material. In this work, anodic porous alumina supported on Al is found to exhibit significant softening during *in situ* nanoindentation with anodization processing. Compared with *ex situ* nanoindentation without anodization processing, the *in situ* hardness measured on the alumina is found to be much lower, when the estimated maximum stress underneath the indenter is exerted on the metal/oxide (m/o) interface at the bottom of the oxide. Numerical calculation reveals that a high electric field exists across the nanometrically thin barrier layer where the electrochemical reactions mainly take place. In microindentation with a flat punch, *in situ* softening is also observed, but no significant difference in the deformation of the oxide and the Al substrate between *in situ* and *ex situ* cases can be observed from cross-sectional transmission electron microscopy examination. The evidence, therefore, indicates that the observed *in situ* softening is due to a combination of high compression stress and electric field acting near the m/o interface, and it is likely that such conditions enhance Al ionization at the m/o interface, thus causing the m/o interface to move faster into the Al substrate under the *in situ* condition. © *2013 AIP Publishing LLC*. [http://dx.doi.org/10.1063/1.4803865]

I. INTRODUCTION

Metals such as aluminum and titanium can form a porous anodic oxide layer on the surface with a quasi-hexagonal arrangement of the nano-pore-channels during anodization.[1–5] Such a form of oxide has previously been used as protective layers against corrosion,[6] and recently been extensively employed as templates for the fabrication of nanomaterials with regular nanoelement arrays for applications including optics,[7] electronics,[8] magnetic memories,[9] biodevices,[10] and so on. The mechanical behavior of these porous oxides is also interesting and important. For example, Xia *et al*. found that when porous alumina was indented, the nanopores collapsed in a shear-band deformation mode rather than by crack formation and propagation in the structure, suggesting that the material can have multi-axial damage tolerance where the pores greatly improve the material's toughness.[11,12] Ng and Ngan demonstrated that the hardness of porous alumina increases significantly with the regularity of the porous pattern.[13–16]

However, in these previous investigations, the mechanical tests performed were all *ex situ* after the anodic porous alumina has already been fabricated by anodization. *In situ* mechanical tests during the growth of the oxide by anodization would be an interesting experiment to perform, since the mechanical stress and electrochemical reactions involved may exhibit coupling effects which have not been revealed before. In this paper, we carried out *in situ* nanoindentation on anodic porous alumina during anodization of Al in a specially designed electrochemical cell. For comparison, *ex situ* nanoindentation with the anodic current switched off was also carried out under comparable conditions. A novel softening effect during *in situ* nanoindentation compared with the *ex situ* case was found. In the following, after reporting the experiments and results, possible reasons for the *in situ* softening are suggested and analyzed.

II. EXPERIMENTAL METHOD

A. Aluminium pre-treatment

99.99% pure aluminum foils were used for the nanoindentation tests. The Al specimens were cut into disks of 1 in. in diameter and 1 mm in thickness. Before testing, the specimens were first annealed under a vacuum of $\sim 10^{-5}$ Torr at 500 °C for 48 h, then mechanically polished with 1200, 2400, 4000 grit SiC sandpapers and 6 μm, 1 μm diamond pastes in succession, and finally electropolished in a mixture solution of $HClO_4$ (60% wt.) and C_2H_5OH in 1:4 ratio by volume under 20 V at about −10 °C for 2 min. The final grain size as measured by electron back-scatter diffraction (EBSD) was about 1 mm.

B. Electrochemical cell setup

To enable anodization to be carried out in the nanoindentation platform, a small cylindrical electrochemical cell was made from polymethyl methacrylate to fit into the space between the sample stage and the transducer of the nanoindenter, as shown in Fig. 1(a). Here, a copper plate connected to an outside power supply was used to support the aluminum disk which acted as the anode. The copper plate was first mounted into an acrylic hot-mounting resin cylinder of 1 in. in diameter, and then the cylindrical assembly was

[a]Author to whom correspondence should be addressed. Electronic mail: chuan.cheng.research@gmail.com.

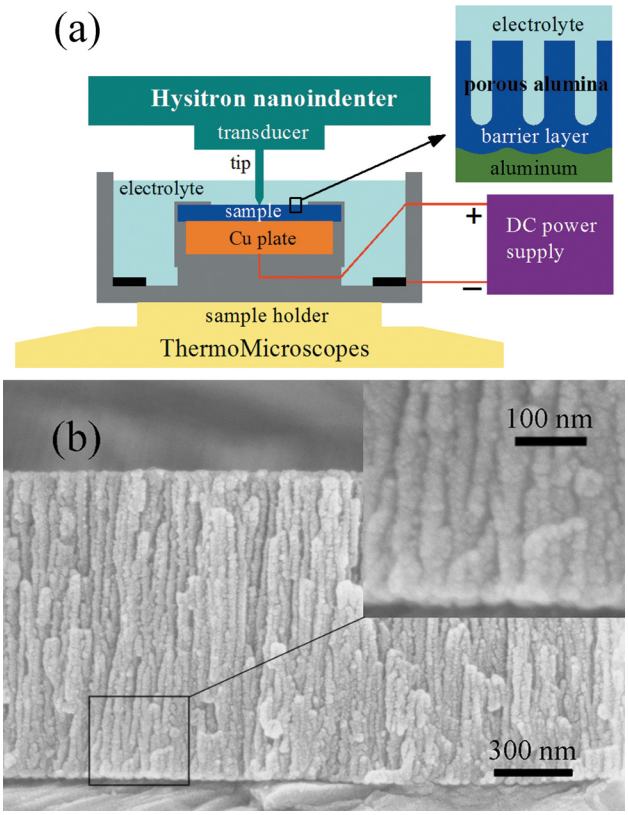

FIG. 1. (a) Schematic of experimental setup for nanoindentation on anodic porous alumina. (b) Cross-section view of anodic porous alumina formed during nanoindentation under the anodization condition of 20 V, 0.2M $H_2C_2O_4$, room temperature, and 21.5 min.

attached to the bottom center of the cell. The Al specimen was attached to the copper plate using conductive epoxy, and then the circular rim between the Al specimen and the cylinder was covered with a flexible rubber sleeve which was about 0.1 mm in thickness, so that only the central part of the Al specimen was exposed to the electrolyte. A copper wire hoop was attached to the bottom of the electrochemical cell and connected with the outside power supply to serve as the cathode. The specimen surface was about 2 mm below the free surface of the electrolyte.

C. *In situ* and *ex situ* nanoindentations

Nanoindentation was carried out on a Hysitron TriboScope nanoindenter (Hysitron Inc., Minneapolis, MN) mounted onto a ThermoMicroscopes scanning probe microscope. The indenter has a Berkovich tip designed for use in liquid (Hysitron Inc.). During *in situ* nanoindentation, anodization of Al was conducted in the electrochemical cell under 20 V, 0.2M $H_2C_2O_4$ (oxalic acid) electrolyte at room temperature. Under this condition, as illustrated in the top right of Fig. 1(a), porous-type anodic alumina is formed with nano-sized pore channels growing vertically from the surface towards the Al substrate. The average oxide growth rate is about 0.89 nm s^{-1}, as shown in Fig. 1(b).

In order to have a basis for comparison, *ex situ* nanoindentation was first conducted with the anodic current turned off, so that the indentation was made on the sample immersed in the electrolyte but without anodization processing. Immediately afterwards, *in situ* nanoindentation was conducted on a fresh location about 4 μm away from the previous indent with the current turned on. After this, the current was turned off again for a second round of *ex situ* indentation on another location 4 μm away. The sequence was then repeated. The same load function was used for both *in situ* and *ex situ* nanoindentations, and this consisted of a load ramp at 100 μN s^{-1} followed by a 5 s holding time at the maximum load $P_{max} = 500$ μN. Although we set the duration of each nanoindentation to be 25 s in the load function, in practice, the Hysitron nanoindenter would add 1 s before loading and 4 s after unloading at the zero load, so that the real indentation period was 30 s. Both the loading and unloading stages have a 5 s holding segment at 10% P_{max} for drift correction. The used drift rate is the average of two drift rates measured from the two 5 s holding segments.

D. *In situ* and *ex situ* microindentations

In addition to nanoindentation with a Berkovich diamond tip, microindentation was also carried out on a Buehler Micromat 2100 hardness tester equipped with a diamond flat punch tip with diameter of ~20 μm, which was made from a previous Vickers tip by focused ion beam (FIB) milling in a Quanta 200 3D dual beam FIB/Scanning electron microscopy (SEM) system operating at 30 kV ion beam voltage. The loading rate of the microindentation was 19.61 mN s^{-1} with 40 s (or 99 s) holding at $P_{max} = 98.07$ mN. Anodization was conducted under 60 V, 0.05M $H_2C_2O_4$ at room temperature in the same electrochemical cell (Sec. II B). For example, after anodization for 300 s, the anodic current was turned off and then *ex situ* microindentation was conducted without anodization processing. Immediately after that, *in situ* microindentation with anodic current on was conducted at a position about 100 μm away from the *ex situ* impression. After that, the current was turned off and the indented specimen was removed from the electrochemical cell for characterization. The indented alumina was formed on the same (001) oriented Al grain, as detected by EBSD scanning of the Al both before anodization and after anodization/indentation by selectively dissolving the formed alumina on top, in a mixed solution of H_2CrO_4, H_3PO_4, and H_2O at 1.8:6:92.2 by weight at 60 °C.

E. Microscopic characterization

SEM was carried out in a LEO 1530 field-emission microscope in order to observe the nanoindentation impressions. Cross-sections of the microindentation impressions were observed by transmission electron microscopy (TEM) carried out in a Philips Tecnai microscope operating at 200 kV. Cross-sectional TEM thin foils were cut from similar positions from the samples, with their long directions parallel to the [010] surface normal and the [101] tangential direction on the surface of the substrate Al grain, for both *ex situ* and *in situ* impressions, by FIB milling with the current varied from 7 nA for initial coarse milling to 0.3 nA for final fine milling. The orientation of the Al substrate was maintained the same, so that comparable diffraction conditions could be achieved in the TEM. Before cutting the TEM

samples, the targeted area was deposited with a tungsten layer about 5 μm thick to protect the porous alumina underneath.

III. RESULTS AND DISCUSSION

A. Softening during *in situ* indentation

Ex situ nanoindentation with anodic current off and *in situ* nanoindentation with current on were performed alternatively as described in Sec. II. After anodizing for 90 s, the current was turned off, and then *ex situ* nanoindentation was performed to obtain the impression shown in Fig. 2(a): 90 s. After that, the anodizing current was turned on, and *in situ* nanoindentation was performed to obtain the impression as shown in Fig. 2(b): 90+ s, with the anodization time reported as 90+ s, where the "+" means that the anodization was still on-going during the *in situ* nanoindentation. This implies that the *in situ* indentation at 90+ s was performed on a slightly thicker oxide than the last *ex situ* indentation at 90 s. Although a thicker oxide was indented in the *in situ* case, it is obvious that the resultant impression in Fig. 2(b): 90+ s is much larger than the *ex situ* one in Fig. 2(a): 90 s, which implies a smaller hardness in the former. In Fig. 2(b): 90+ s, the fracture of alumina during indentation is reflected as the pop-in of the load-depth curve shown in Fig. 2(d): 90+ s. As the anodization time increases, the thickness of anodic alumina also increases, and this is accompanied by a gradual reduction of the indent area for both *ex situ* (Fig. 2(a)) and *in situ* tests (Fig. 2(b)), but at the same time point the *in situ* nanoindent is always larger than that of the *ex situ* indents. Generally speaking, for indentation performed on a supported film, if the indentation depth to film thickness ratio is larger than 0.1, the substrate may influence the measured hardness.[17] Here, the contact depth (h_c) is obtained from the load-depth curves in Figs. 2(c) and 2(d), and the alumina thickness was evaluated as the product of the measured average oxide growth rate ($\sim$0.89 nm s^{-1}) and the total anodization time, counted as the sum of the durations when the anodization current was switched on, from the beginning of the experiment. From Fig. 2(e), the h_c to oxide thickness ratio decreases quickly from 2.86 (*in situ* 60+ s) and 2.28 (*ex situ* 60 s) to 0.17 (*in situ* 330+ s) and 0.16 (*ex situ* 330 s), which are all larger than 0.1. The reduction of the indent area as the oxide grows in thickness as seen in Figs. 2(a) and 2(b) indicates that the measured hardness is that for the oxide/Al composite, but the role of the Al substrate decreases quickly as the oxide thickens with increasing anodization time. The hardness difference between *in situ* and *ex situ* tests is reflected more clearly in the load-depth curves as shown in Figs. 2(c) and 2(d). The maximum and residual depths in the *in situ* indentation curves are all much larger than the corresponding *ex situ* cases, indicating that the hardness of the oxide/Al composite system under the *in situ* condition is much lower than that in the *ex situ* condition. In addition, within the same anodization time intervals, such as 90 to 150 s, or 210 to 270 s, the maximum or residual depth decreases much faster for the *in situ* case than the *ex situ* case. This is in accordance with the trend of the contact depth as shown in Fig. 2(e), implying that the influence of the Al substrate reduces faster in the *in situ* case.

The areas A_{SEM} of the indents as measured from the SEM micrographs were used to calculate the hardness of the sample according to

$$H_{SEM} = \frac{P_{\max}}{A_{SEM}}, \tag{1}$$

where $P_{\max}$ is the maximum load. The hardness of the sample was also calculated by the Oliver-Pharr method[18,19]

$$H_{O-P} = \frac{P_{\max}}{A_c(h_c)}, \tag{2}$$

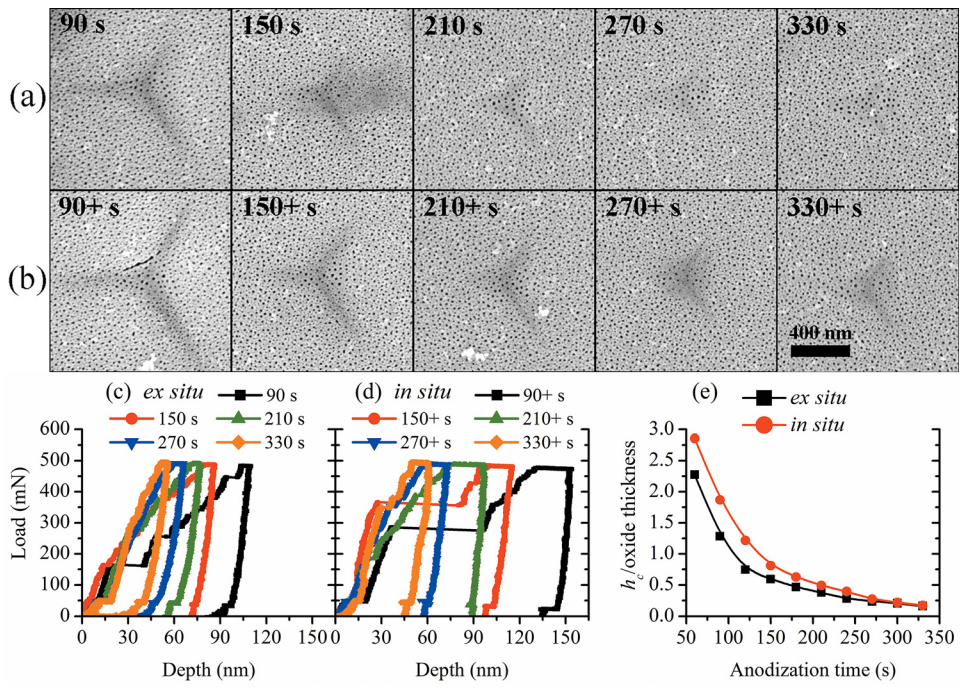

FIG. 2. (a) SEM of *ex situ* nanoindentation impressions at anodization time of 90 s, 150 s, 210 s, 270 s, and 330 s, respectively. (b) SEM of *in situ* nanoindentation impressions at anodization time of 90+ s, 150+ s, 210+ s, 270+ s, and 330+ s, respectively, where "+" means anodization is on-going during the *in situ* nanoindentation. (c) and (d) Load-depth curves corresponding to impressions in (a) and (b), respectively. (e) Contact depth (h_c) to oxide thickness ratio vs anodization time. All SEM figures have the same magnification.

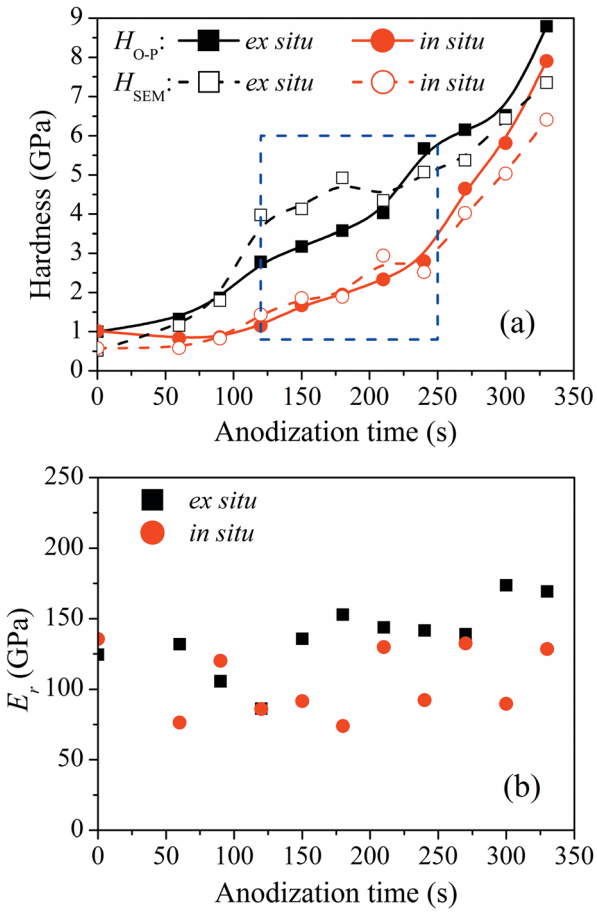

FIG. 3. (a) Hardness vs anodization time, where solid symbols and hollow symbols represent H_{SEM} and H_{O-P}, respectively. The dashed blue contour indicates an anodization time zone when the hardness difference between *ex situ* and *in situ* nanoindentations is relatively large compared with other anodization time. (b) Measured reduced modulus E_r vs anodization time.

where A_c is the contact area, which is a function of h_c depending on the tip geometry.[17] The H_{SEM} and H_{O-P} estimates of the hardness are plotted as a function of the anodization time in Fig. 3(a). Under both the *in situ* and *ex situ* conditions, the trends of the H_{O-P} and H_{SEM} on increasing anodization time are in accordance with each other. Although some discrepancies exist between the H_{SEM} and H_{O-P} values and these may be due to the SEM measured indent areas A_{SEM} not reflecting the porous structure of the oxide,[15] both methods of calculation demonstrate that the *in situ* nanoindentation hardness is lower than the corresponding *ex situ* value at comparable anodization times. Moreover, the hardness difference between the *in situ* and *ex situ* cases is very small at the beginning stage ($t < 60$ s) or the end stage ($t > 300$ s) of anodization, but during an intermediate stage of $120\text{ s} < t < 250\text{ s}$, as indicated by the blue-dashed box in Fig. 3(a), the *in situ* hardness is significantly lower than the *ex situ* hardness. The corresponding porous alumina thickness of the intermediate stage is about 107 to 223 nm, and the h_c to oxide thickness ratio (Fig. 2(e)) is about 1.22 to 0.39 for the *in situ* case, and 0.74 to 0.27 for the *ex situ* case. In addition, for both *ex situ* and *in situ* conditions, the measured hardness increases from the value for pure Al (~0.6 GPa)[20] towards that for pure porous alumina (~8 GPa)[11] as the anodization time increases. This implies the increasing contribution of the porous alumina layer to the measured hardness as the oxide thickens during anodization. Fig. 3(b) shows the reduced modulus E_r measured from load-depth curves using the Oliver-Pharr method.[18,19] Although E_r values do not vary much with anodization time for both *in situ* and *ex situ* cases, the E_r values of the *in situ* case are generally 32 GPa lower than that of *ex situ* case. Here, the average *ex situ* E_r is 137 GPa, which is close to previous results, such as the 140 GPa by Xia *et al.*[11] or 130 ± 10 GPa by Ko *et al.*[21] But no *in situ* E_r value has been reported before.

At the same anodization time, the key difference between *in situ* and *ex situ* nanoindentations is whether the anodization current is on or off. Thus, the softening observed during *in situ* nanoindentation has to be a result of the anodization current which passes through the specimen during the test. However, since the material system indented comprises a porous alumina layer on top and an Al substrate below, it is important to understand which component softens during anodization. From contact mechanics, the maximum shear stress underneath the indenter is $\tau_{max} \approx 0.46H$, where H is the hardness, and this occurs at a depth $h_{\tau\,max}$ approximately 0.48 times the contact radius a_c below the sample surface.[22,23] The contact radius a_c can be estimated from the relationship $A_c = \pi a_c^2 \approx 24.5 h_c^2$ for the a Berkovich tip, and so the position of τ_{max} can be estimated as

$$h_{\tau\,max} \approx 1.34 h_c. \tag{3}$$

The variation of $h_{\tau\,max}$ with the anodization time is shown in Fig. 4(a). Also shown in Fig. 4(a) is the depth of the metal/oxide (m/o) interface below the oxide's top surface, which appears as a sloping band with the same thickness (26 nm, under 20 V) as the oxide barrier layer just above the m/o interface. Because the m/o interface is always in contact with the Al substrate, its position can be obtained from the porous oxide's thickness at each anodization time. From Fig. 4(a), there is a region of anodization time ($120\text{ s} < t < 250\text{ s}$, labeled with blue dashed square) in which the most highly stressed location approximately overlaps with the m/o interface. This region coincides with the same time region plotted in Fig. 3(a) (also labeled with blue dash square), during which the most significant hardness reduction is observed during *in situ* nanoindentation compared with *ex situ* nanoindentation. This suggests whenever the τ_{max} is exerted close to the m/o interface, a significant reduction of *in situ* hardness compared with *ex situ* hardness is detected by nanoindentation. The results here suggest that, with the anodization current on, softening mainly happens near the m/o interface.

B. Possible explanations of the *in situ* softening

The above softening during *in situ* indentation may be due to a number of reasons, which are discussed below.

1. Electric-field assisted softening of oxide

During anodization, an ultra-high electric field is expected to exist across the oxide barrier layer,[24,25] which is a thin scallop shaped layer located along the m/o interface

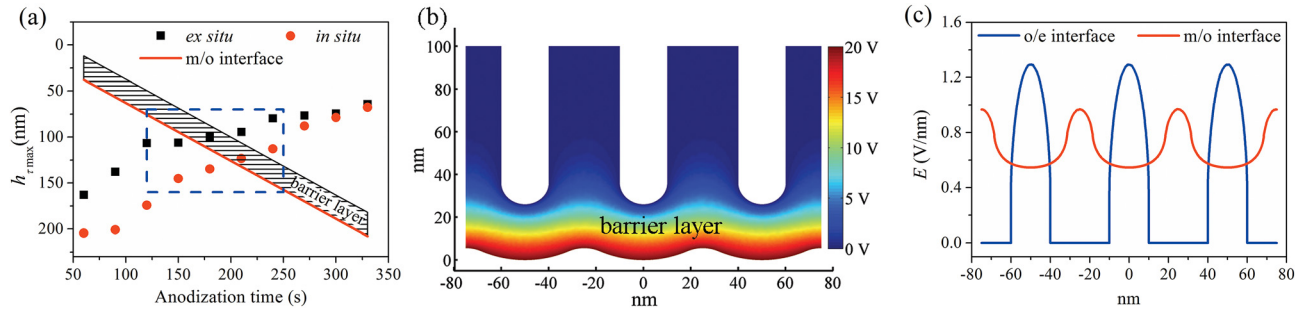

FIG. 4. (a) Maximum shear stress position and m/o interface position below the sample surface vs anodization time. (b) Electric potential distribution in porous alumina during *in situ* nanoindentation. (c) Electric field intensity along oxide/electrolyte (o/e) and metal/oxide (m/o) interfaces, respectively.

with thickness proportional to the anodization voltage.[26] We have performed an analysis to predict the order of magnitude of the electric field within the oxide barrier layer during anodization. Following Parkhutik and Shershulsky[27] and Singh *et al.*,[28] when space charge within the oxide and double layer effects at the interfaces are neglected, the electric potential φ within the anodic alumina is governed by the Laplace equation

$$\nabla^2\varphi = 0, \tag{4}$$

where $\nabla = (\partial/\partial x, \partial/\partial y)$ for the present two-dimensional (2-D) considerations. Equation (4) was solved by the finite-element method within a 2-D domain, which represents the anodic alumina used in the nanoindentation. The boundary conditions are $\varphi = 0$ at the o/e interface, $\varphi = 20\,\mathrm{V}$ (the anodization voltage) at the m/o interface, and $\mathbf{n}\cdot\nabla\varphi = 0$ on the left and right sides, where $\mathbf{n}$ is the outward normal unit vector of the two sides of the domain. Numerical calculation was performed with a computer code developed from the MATLAB PDE toolbox.[29] Details on the simulation of the real-time growth of porous alumina during anodization can be found in our previous paper.[24] As shown in Fig. 4(b), the electric potential drop mainly concentrates within the barrier layer, while within the finger-like pore-walls the drop is very weak. Accordingly, in Fig. 4(c), the electric field intensity $E = |\nabla\varphi|$ along o/e interface can reach a maximum value of $1.3\,\mathrm{V\,nm^{-1}}$ at the pore bottom, while along m/o interface, a high value of $1.0\,\mathrm{V\,nm^{-1}}$ occurs at the ridges between two neighboring pores. Under such a high electric field intensity, high migration rates of Al^{3+} and O^{2-} ions across the barrier layer may happen,[30,31] as the density of mobile ions was found to be exponentially proportional to the electric field intensity.[30] Houser and Hebert theoretically proposed that during anodization, Al^{3+} and O^{2-} ions are transported by coupled electrical migration and viscous flow, and oxide flow arises near the oxide/electrolyte (o/e) interface at the pores' bottom.[32] If oxide flow really exists, the mechanical strength of the oxide barrier layer should be greatly reduced, compared with the situation without anodization on-going.

2. Enhancement of electrochemical reactions at m/o interface

A second consequence of the ultra-high electric field across the oxide barrier layer is that electrochemical reactions at the m/o interface may be greatly enhanced.[24,30,32] At the m/o interface, Al ions are produced from Al substrate by ionization

$$\mathrm{Al_{(m)} \rightarrow Al^{3+}_{(ox)} + 3e^-}. \tag{5}$$

One portion of such Al^{3+} ions will form new oxide at the m/o interface according to

$$\mathrm{2Al^{3+}_{(ox)} + 3O^{2-}_{(ox)} \rightarrow Al_2O_{3(ox)}} \tag{6}$$

and the rest (~30%) of Al^{3+} will migrate across the barrier layer and then are ejected into the electrolyte without oxide formation.[33,34] The needed O^{2-} ions in Eq. (6) come from the water decomposition at the o/e interface[32] and then migration across the barrier layer to reach the m/o interface. During *in situ* indentation, these reactions at the m/o interface may be further enhanced, causing the m/o interface to advance more quickly into the Al substrate and thus a softening effect. This possibility will be further discussed later.

3. Enhancement of dislocation activities in Al substrate

The oxidation reaction in Eq. (6), which takes place at the m/o interface, is accompanied by volume expansion.[35,36] The Pilling-Bedworth ratio[35,36] after considering the 30% loss of Al^{3+} ions is

$$\frac{(26.98\,\mathrm{g} + 1.5 \times 15.99\,\mathrm{g})/3.0\,\mathrm{g\,cm^{-3}}}{26.98\,\mathrm{g}/2.7\,\mathrm{g\,cm^{-3}}} \times (1 - 0.3) = 1.19, \tag{7}$$

which means 19% volume increase. This implies that large stresses may be created during *in situ* indentation at the m/o interface,[36] which may facilitate the deformation of the oxide barrier layer as well as the Al substrate just below the barrier layer, since the hardness of Al metal is more than 10 times smaller than that of the anodic alumina oxide.[11,20] Moreover, as the electric current passes through the Al substrate, dislocation activities within it may be enhanced, resulting in softening compared with the situation without current passing.

C. TEM examination of deformation of oxide and Al substrate

Explanation in Secs. III B 1 and III B 3 involves enhanced deformation of the oxide and dislocation plasticity at the Al substrate, respectively, and to examine whether these can actually occur, we performed *in situ* microindentation experiments on the anodic porous alumina during anodization using a flat punch indenter as shown in Fig. 5(a). *Ex situ* microindentation without anodization processing was also conducted for comparison. The anodization voltage was selected to be 60 V in order to obtain a relatively thicker barrier layer for better observation, according to the linear relationship between anodization voltage and barrier layer thickness.[26] The electrolyte was 0.05M $H_2C_2O_4$ at room temperature. After anodization for 300 s, the current was turned off, and then *ex situ* indentation was conducted to obtain the impression shown on the left hand side of Fig. 5(b). Immediately after that, *in situ* indentation with anodic current on was conducted to obtain the impression shown on the right hand side of Fig. 5(b). These two impressions were separated about 100 μm apart, but they were on the oxide formed on the same (001) oriented Al grain, as confirmed by EBSD after selectively dissolving the anodic alumina on top. To observe the cross-sectional view of the impressions, TEM samples were cut by FIB milling at similar positions at the edge of each impression, as marked by black rectangles in Fig. 5(b). Figs. 5(c) and 5(d) show the TEM images of the cross-sectional view of the *ex situ* and *in situ* impressions, respectively. The tube like feathers were the anodic porous alumina, with the Al substrate below and the tungsten protective layer (black) on top. The residual depth for the *ex situ* indent is measured to be 2.45 μm, which is about 390 nm smaller than the 2.84 μm of the *in situ* indent. This indicates that the *in situ* hardness is smaller than the *ex situ* hardness, which is in accordance with the nanoindentation results described in Sec. III A. From Figs. 5(c) and 5(d), plastic deformation mainly happened in the Al substrate below the alumina, while in the alumina brittle fracture happened only at the edge of each impression, and the reduction in the oxide thickness within the indented part relative to immediately outside the indent is rather mild, i.e., from 0.92 μm to 0.80 μm (a reduction by 120 nm) for the *ex situ* case, and from 1.03 μm to 0.72 μm (a reduction by 310 nm) for the *in situ* case, compared to indent depths between 2 and 3 μm. This situation is mainly due to the large difference in hardness between alumina and Al substrate, and in any case, the changes in thickness of the porous oxide layer between the *in situ* and *ex situ* cases are not large enough to account for the difference in indentation depths between the two cases.

Figures 5(e) and 5(f) show the cross-sectional view under the impressions near the oxide barrier layer in the *ex situ* and *in situ* cases, respectively. Again, no significant change in the thickness of the oxide barrier layer can be observed between the two cases; the barrier layer thicknesses for both the *ex situ* and *in situ* cases are measured to be 59 ± 1 nm, which is almost the same as that outside the indentation impressions. This may be because the Al substrate is very soft compared to the hardness of oxide barrier layer,

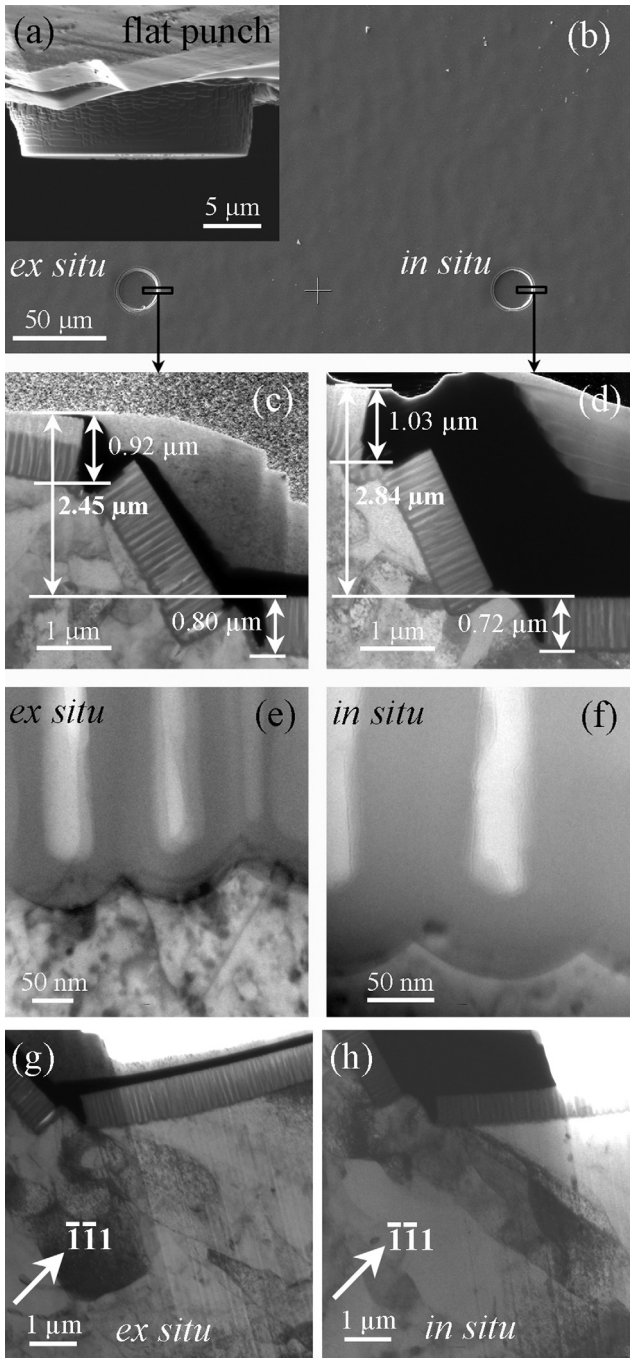

FIG. 5. (a) The diamond flat punch used in the microindentation. (b) Top view of the indentation impressions obtained by *ex situ* indentation at t = 300 s (left hand side) and *in situ* indentation at t = 300+ s (right hand side). The holding time is 40 s at the maximum load of 98.07 mN. TEM cross-sectional view of (c), (e), and (g) *ex situ* and (d), (f), and (h) *in situ* impressions. (c) and (d) The edges of impressions; (e) and (f) the m/o interface at the barrier layer of porous alumina underneath the impressions; (g) and (h) the Al substrate underneath the impressions. TEM images were taken at $\boldsymbol{g} = (\bar{1}\bar{1}1)$ near [101] pole for (g) and (h).

even with electrochemical reactions and ion migration taking place under the *in situ* case. Thus, the softening observed during *in situ* indentation is not due to a difference in the deformation of the oxide barrier layer of porous alumina. Figs. 5(g) and 5(h) show the deformation microstructures of the Al substrate in the *ex situ* and *in situ* cases, respectively, under the same electron diffraction condition $\boldsymbol{g} = (\bar{1}\bar{1}1)$.

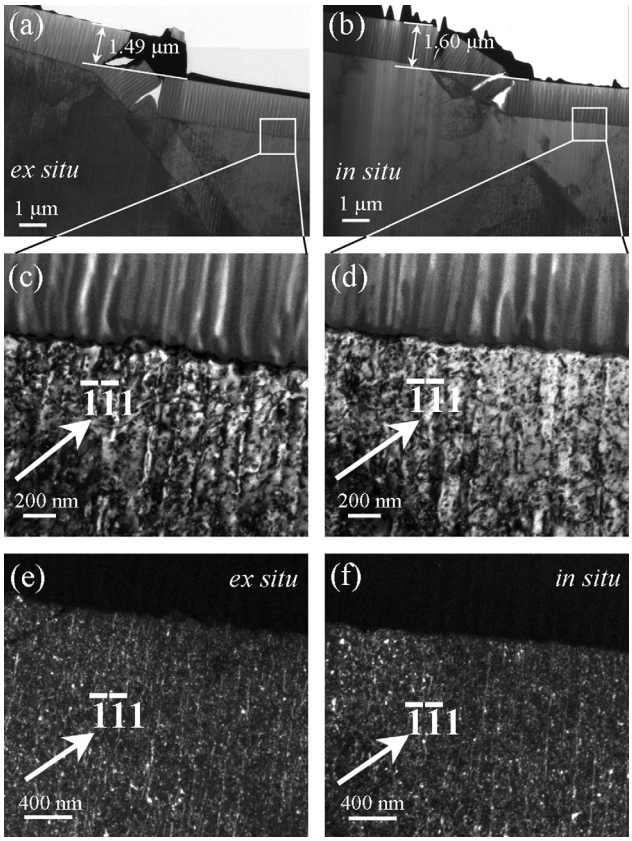

FIG. 6. (a) and (b) TEM cross-sectional view of flat punch microindentation impressions performed at 500 s and 500+ s under *ex situ* and *in situ* conditions, respectively. The holding time was 99 s at the maximum load of 98.07 mN. (c) and (d) Bright-field and (e) and (f) dark-field TEM cross-sectional view of impressions around the metal/oxide interface underneath the (c) and (e) *ex situ* and (d) and (f) *in situ* impressions. All TEM images were taken at $\boldsymbol{g} = (\bar{1}\bar{1}1)$ near [101] pole for (c)–(f).

In both cases, dense dislocation networks and subgrain formation can be seen in the Al substrate just underneath the indent, and there is no compelling evidence to indicate that dislocation activities in the Al substrate are more intensive in the *in situ* case than the *ex situ* case.

Figure 6 shows the TEM cross-sectional views of another pair of *ex situ* and *in situ* flat-punch microindentation impressions made on another specimen. This time, the holding time at the P_{max} was 99 s and before indentation the anodization had been on-going for 500 s, but apart from these other conditions are the same as Fig. 5. As similar to Fig. 5, the *in situ* softening also occurred during microindentation, and from Figs. 6(c) and 6(d), significant deformation of the oxide barrier layer at the bottom of the porous alumina is also not observed for both the *ex situ* and *in situ* cases. From Figs. 6(c)–6(f), under the same electron diffraction condition of $\boldsymbol{g} = (\bar{1}\bar{1}1)$ near [101] pole, the dislocation density within the Al substrate, measured as the inverse-square of the average dislocation spacing, is of the same order of magnitude of 10^{15} m/m^3 in both the *ex situ* and *in situ* cases. Thus, Fig. 6 also indicates the *in situ* softening is neither due to the softening of the oxide barrier layer nor the Al substrate just underneath the *in situ* indented porous alumina.

D. Enhancement of electrochemical reactions at the m/o interface by high electric-field and stress

The proposed mechanisms for the *in situ* softening in Sec. III B 1 and III B 3 have now been ruled out by the above TEM results. Recalling that in Fig. 4(a), *in situ* softening is significant only when the maximum stress under the impression is exerted at around the m/o interface. Thus, as discussed in Sec. III B 2, the reason for the *in situ* softening is evidently related to the enhancement of certain electrochemical reactions that happen at the m/o interface, by the presence of a combination of high stress and electric-field there. On the one hand, oxide formation in Eq. (6) would lead to propagation of the m/o interface into the Al substrate, but this reaction should not be enhanced by a compressive mechanical stress because of the volume expansion due to oxidization. A compressive mechanical stress would tend to suppress the volume expansion, so the oxidation reaction can only be retarded, rather than enhanced. For example in Fig. 5(d), during the *in situ* microindentation, a compression stress is exerted on the alumina during its growth by Eq. (6), while the Al substrate on either side, but not underneath the impression, should be subjected to tension due to the volume expansion of the oxide above. The oxide thickness underneath the impression is about 0.72 μm, which is 310 nm smaller than the thickness just outside the impression ($\sim$1.03 μm). This large difference was produced within a short microindentation duration of 50 s, thus the retarding effect of a compressive stress on the oxidation reaction is rather large. Similarly, for the *ex situ* impression shown in Fig. 5(c), the oxide thickness within the impression region ($\sim$0.8 μm) is only about 120 nm smaller than that just outside the impression ($\sim$0.92 μm). This difference is much smaller than the *in situ* case of 310 nm, as only the residual compression and tensile stresses play roles in the alumina growth after the *ex situ* impression has already been formed.

On the other hand, under *in situ* indentation, the ionization reaction of Al in Eq. (5) can be promoted by both a high electric field and compression stress. Underneath an *in situ* impression, high compressive stresses are present near the m/o interface due to the volume expansion accompanying oxidation in Eq. (6), and also the indentation force. Therefore, when the maximum stress position of the indentation field overlaps with the m/o interface (Fig. 4(a)), the ionization reaction in Eq. (5) may be enhanced there by the compression stress, since Al atom ionized will be pumped across the oxide barrier layer into the electrolyte by the high electric field and stress in the barrier layer. In this way, Eq. (5) effectively serves as a relief mechanism for the compressive stress in the *in situ* case, and such a stress relief mechanism is not present in the *ex situ* condition. Therefore, during *in situ* indentation, Al atoms in the substrate are continuously lost into the electrolyte, while the remaining substrate also undergoes plastic deformation, but in the *ex situ* case, only plastic deformation can happen. As a result, the m/o interface in the *in situ* case should advance faster than the *ex situ* case, especially during the holding at the P_{max} of microindentation, and so the *in situ* indent depth becomes deeper, corresponding to the softening observed.

No matter what the actual mechanism is, the chemo-mechanical softening observed from the present *in situ* indentation experiments is a novel phenomenon which may find applications in the future, including as an enhanced means for micro-stamping and micro-surface texturing of thin oxide films. The combined effects of high electric field and mechanical stresses on electrochemical reactions as well as plastic deformation near nano-scale interfaces are also an open area deserving more investigations in the future.

IV. CONCLUSIONS

In situ nanoindentation hardness of anodic porous alumina supported on Al substrate during anodization is found to be significantly smaller than the *ex situ* hardness, in a window of anodization time within which the estimated position of the maximum stress in the indentation field overlaps with the position of the metal/oxide (m/o) interface. Numerical simulations show that during anodization, the electric field intensity in the barrier layer is at a high magnitude of $\sim 1\,\mathrm{V\,nm^{-1}}$. Cross-sectional TEM examination reveals that dislocation activities in the Al substrate, as well as the thickness of the oxide barrier layer, are similar in both the *in situ* and *ex situ* indentation cases. The total oxide thickness in the *in situ* case is somewhat smaller, but the difference with the *ex situ* case is still not large enough to explain the softening observed. Summing up the evidence, the observed softening during *in situ* indentation is not due to enhanced deformation of the formed oxide or dislocation activities in the Al substrate, but is likely the result of enhanced Al ionization at the m/o interface, due to a combined high electric field and compressive stress there.

ACKNOWLEDGMENTS

The work described in this paper was supported by grants from the Research Grants Council (Project No. HKU7159/10 E), as well as from the University Grants Committee (Project No. SEG-HKU06) of the Hong Kong Special Administration Region, P.R. China.

[1]G. E. Thompson and G. C. Wood, Nature **290**, 230 (1981).
[2]H. Masuda and K. Fukuda, Science **268**, 1466 (1995).
[3]W. Lee, R. Ji, U. Gösele, and K. Nielsch, Nature Mater. **5**, 741 (2006).
[4]Z. Su and W. Zhou, Adv. Mater. **20**, 3663 (2008).
[5]C. K. Y. Ng and A. H. W. Ngan, Chem. Mater. **23**, 5264 (2011).
[6]G. E. Thompson, Thin Solid Films **297**, 192 (1997).
[7]H. Masuda, M. Yamada, F. Matsumoto, S. Yokoyama, S. Mashiko, M. Nakao, and K. Nishio, Adv. Mater. **18**, 213 (2006).
[8]W. B. Choi, J. U. Chu, K. S. Jeong, E. J. Bae, J. W. Lee, J. J. Kim, and J. O. Lee, Appl. Phys. Lett. **79**, 3696 (2001).
[9]W. Lee, H. Han, A. Lotnyk, M. A. Schubert, S. Senz, M. Alexe, D. Hesse, S. Baik, and U. Gösele, Nat. Nanotechnol. **3**, 402 (2008).
[10]F. Matsumoto, K. Nishio, and H. Masuda, Adv. Mater. **16**, 2105 (2004).
[11]Z. Xia, L. Riester, B. W. Sheldon, W. A. Curtin, J. Liang, A. Yin, and J. M. Xu, Rev. Adv. Mater. Sci. **6**, 131 (2004).
[12]Z. Xia, L. Riester, W. A. Curtin, H. Li, B. W. Sheldon, J. Liang, B. Chang, and J. M. Xu, Acta Mater. **52**, 931 (2004).
[13]K. Y. Ng and A. H. W. Ngan, Scr. Mater. **66**, 439 (2012).
[14]K. Y. Ng, L. Zuo, and A. H. W. Ngan, Scr. Mater. **61**, 955 (2009).
[15]K. Y. Ng, Y. Lin, and A. H. W. Ngan, Acta Mater. **57**, 2710 (2009).
[16]S. Wang, A. H. W. Ngan, and K. Y. Ng, Scr. Mater. **67**, 360 (2012).
[17]A. C. Fischer-Cripps, *Nanoindentation*, 2nd ed. (Springer, New York, 2004).
[18]W. C. Oliver and G. M. Pharr, J. Mater. Res. **7**, 1564 (1992).
[19]W. C. Oliver and G. M. Pharr, J. Mater. Res. **19**, 3 (2004).
[20]N. G. Chechenin, J. Bottiger, and J. P. Krog, Thin Solid Films **261**, 228 (1995).
[21]S. Ko, D. Lee, S. Jee, H. Park, K. Lee, and W. Hwang, Thin Solid Films **515**, 1932 (2006).
[22]A. Barnoush and H. Vehoff, Scr. Mater. **58**, 747 (2008).
[23]K. L. Johnson, *Contact Mechanics* (Cambridge University Press, Cambridge, 2003).
[24]C. Cheng and A. H. W. Ngan, Electrochim. Acta **56**, 9998 (2011).
[25]C. Cheng, K. Y. Ng, and A. H. W. Ngan, AIP Adv. **1**, 042113 (2011).
[26]J. P. O'Sullivan and G. C. Wood, Proc. R. Soc. London, Ser. A **317**, 511 (1970).
[27]V. P. Parkhutik and V. I. Shershulsky, J. Phys. D: Appl. Phys. **25**, 1258 (1992).
[28]G. K. Singh, A. A. Golovin, and I. S. Aranson, Phys. Rev. B **73**, 205422 (2006).
[29]MATLAB R2009a, version 7.8.0.347, The Mathworks Inc., 2009.
[30]M. M. Lohrengel, Mater. Sci. Eng. R. **11**, 243 (1993).
[31]J. W. Diggle, T. C. Downie, and C. W. Goulding, Chem. Rev. **69**, 365 (1969).
[32]J. E. Houser and K. R. Hebert, Nature Mater. **8**, 415 (2009).
[33]J. Siejka and C. Ortega, J. Electrochem. Soc. **124**, 883 (1977).
[34]C. Cherki and J. Siejka, J. Electrochem. Soc. **120**, 784 (1973).
[35]R. E. Smallman and A. H. W. Ngan, *Physical Metallurgy and Advanced Materials* (Elsevier, Amsterdam, 2007).
[36]F. Li, L. Zhang, and R. M. Metzger, Chem. Mater. **10**, 2470 (1998).